Journal of Ceramic Processing Research. Vol. 25, No. 4, pp. 563~571 (2024)
(Received 17 March 2024, Received in revised form 5 June 2024, Accepted 25 June 2024)
https://doi.org/10.36410/jcpr.2024.25.4.563

J O U R N A L O F
Ceramic Processing Research

Design optimization of synthesis of composite calcium hydroxide loaded with ZnO and Ag nanoparticles as an antibacterial Agent

Mohsen Safaei,[a,b] Somaye Moloudi,[c] Razieh Souri,[b] Amir Sabzi,[b] Ling Shing Wong[d] and Roohollah Sharifi[b,e,*]
[a]*Division of Dental Biomaterials, School of Dentistry, Kermanshah University of Medical Sciences, Kermanshah, Iran*
[b]*Advanced Dental Sciences and Technology Research Center, School of Dentistry, Kermanshah University of Medical Sciences, Kermanshah, Iran*
[c]*Students Research Committee, Kermanshah University of Medical Sciences, Kermanshah, Iran*
[d]*Faculty of Health and Life Sciences, INTI International University, Nilai 71800, Malaysia*
[e]*Department of Endodontics, School of Dentistry, Kermanshah University of Medical Sciences, Kermanshah, Iran*

Antibiotic resistance has become the major global health hazard that threatens people of all ages. The most important way to reduce infectious diseases in the treatment of the root canal is the elimination of infections caused by the accumulation of bacteria. The objective of this investigation was to enhance the production process of a newly developed nanocomposite composed of calcium hydroxide, zinc oxide, and silver. The intention behind this optimization was to achieve the utmost effectiveness in combating *Enterococcus faecalis* infection by exhibiting strong antibacterial properties. To fabricate nanocomposite with the best performance, the effects of three factors of calcium hydroxide ($Ca(OH)_2$), zinc oxide (ZnO) and silver (Ag) nanoparticles (NPs), were investigated in three levels and nine different experiments designed using the Taguchi method. The successful formation of a nanocomposite with desired structural properties was confirmed through various analytical techniques including FTIR, UV-vis, XRD, SEM, EDX, X-Ray Map, TEM, and TGA. The findings indicated that the produced nanocomposite when subjected to the experimental circumstances of calcium hydroxide at a concentration of 50 mg/ml, ZnO at a concentration of 2 mg/ml, and Ag at a concentration of 2 mg/ml, exhibited the most potent antibacterial efficacy (0.26 CFU/ml) against the biofilm of *Enterococcus faecalis*. Due to the favorable antibacterial properties of this nanocomposite, its use as an in-channel drug can lead to more successful root canal treatments.

Keywords: Ceramic nanoparticles, Nanocomposite, Process innovation, Antibiotic resistance, Human health.

Introduction

One of the current concerns of the medical community is the growing prevalence of antibiotic resistance due to inappropriate and arbitrary use of antibiotics. The increasing antibiotic resistance increases treatment costs and prolongs the recovery period, necessitating the search for new compounds with the ability to replace antibiotics [1]. Microorganisms are the cause of pulp and periapical diseases. The main goal of root canal therapy is to remove microorganisms from the root canal [2]. Studies have shown that combining mechanical debridement, root canal establishment, and appropriate washing solutions reduces microorganisms [3]. However, the outcomes of cultivating bacterial specimens originating from the root canal cavity continue to exhibit positivity in numerous instances [4, 5]. *E. faecalis* is a bacterial species that is resistant and persists within the root canal. Its occurrence within this region correlates with a heightened probability of failure in both initial root canal treatment and subsequent re-treatment [3]. Although a considerable amount of research has been dedicated to the development of innovative antimicrobial substances in order to address this issue, the majority of these endeavors were unsuccessful in attaining the intended outcomes owing to the swift degradation and liberation of antibacterial agents [6, 7]. Dental materials can be used for preventive repairs. The four categories of dental materials are metals, ceramics, polymers and composites. Despite recent advances in the properties of these materials, none of these materials have a long shelf life. Ideal description of a hypothetical restorative material due to (1) its biocompatibility, (2) ability to bond continuously to tooth or bone structure, (3) ability to mimic the natural appearance of tooth enamel, dentin, and other tissues, (4) ability to determine properties similar to tooth enamel, dentin and other tissues, and (5) the ability to initiate tissue repair or regeneration of damaged tissues or lost tissues [8].

Due to the high potential of nanoscale materials, many efforts have been made to control their structure and performance. These materials are used in a wide

*Corresponding author:
Tel : +98-833-37296591
Fax: +98-833-38277164
E-mail: roholahsharifi@gmail.com

range of research, including energy conversion devices, photocatalytic activity, and biomedical applications [9].

Calcium hydroxide is used as a common intracanal disinfectant that destroys the cell membrane and protein structure of bacteria by releasing hydroxyl ions and can disinfect the root canal [10, 11]. However, some studies have reported that this substance does not have a favorable effect on the reduction of *E. faecalis* [12, 13]. Therefore, the concomitant use of calcium hydroxide with other antibacterial compounds can be helpful.

Nanoparticles generally refer to small particles ranging from 1 to 100 nm in diameter, which have demonstrated favorable outcomes in the realm of antibacterial treatments owing to their distinctive physical and chemical attributes, encompassing their exceedingly diminutive dimensions, notable surface-to-volume ratio, and augmented chemical responsiveness [14-17]. Nanoparticles possess advantageous antibacterial characteristics, thereby offering a novel approach to the management and prevention of dental infections. The expansive surface area and substantial charge density of NPs afford them the ability to establish heightened interaction with the negatively charged state of bacterial cells, thereby augmenting their antimicrobial efficacy [18, 19].

Zinc oxide (ZnO (as a metal oxide semiconductor, has wide potential applications such as photocatalyst, disinfectant, sensor and solar cells [20, 21]. ZnO and silver (Ag) NPs are between the most widely used and effective antibacterial compounds. Research has demonstrated that ZnO nanoparticles exhibit greater efficacy against Gram-positive bacteria, which encompasses *E. faecalis*, as compared to Gram-negative bacteria [22]. In addition, ZnO reduces *E. faecalis* adhesion by 80-95%. On the other hand, the combination of ZnO NPs with other materials used as intra-canal drugs improves the antibacterial properties of these materials [23]. Silver nanoparticles (Ag NPs) have the capability to adhere to and infiltrate the cellular membranes of both Gram-positive and Gram-negative bacteria, ultimately disturbing cellular operations through the liberation of Ag ions. Consequently, they are employed for the purpose of managing and forestalling the proliferation of drug-resistant microorganisms, as well as impeding the development of biofilms [24]. Previous studies have reported a positive synergistic effect between Ag and ZnO NPs on their antimicrobial activity [25, 26].

In this study, a novel calcium hydroxide/ZnO/Ag nanocomposite was designed and its optimal synthesis conditions were studied with the highest antibacterial activity against *E. faecalis* biofilm.

Materials and Methods

Synthesis of Ag NPs

Solutions comprising silver nitrate ($AgNO_3$) and trisodium citrate dihydrate ($C_6H_5Na_3O_7.2H_2O$) were employed for the synthesis of silver nanoparticles (Ag NPs). To achieve this objective, a 50 ml volume of a 0.01 M solution of $AgNO_3$ was subjected to boiling, followed by the gradual addition of 5 ml of a 1% trisodium citrate ($Na_3C_6H_5O_7$) solution. The resulting mixture was agitated thoroughly to attain a uniform solution, which exhibited a pale yellow hue upon reaching a temperature of 50°C. Subsequently, the solution was extracted from the heated environment and allowed to cool to room temperature. The resulting solution was centrifuged at 5000 rpm 3 times for 15 min to remove impurities [27].

Synthesis of ZnO NPs

In the synthesis of ZnO NPs, 0.83 g of zinc chloride ($ZnCl_2$), 1.19 g of sodium hydroxide (NaOH), and 1.1 g of potassium hydroxide (KOH) were mixed using a molten salt method and placed in an oven at 220 °C for 45 min. The product was then washed 3 times at room temperature to remove impurities using hot distilled water, followed by centrifugation. The precipitate that ensued was subjected to an oven environment with a temperature of 100°C for a duration of 2 hours, ultimately yielding a white powdery substance composed of ZnO nanoparticles [28].

Table 1. Taguchi design of experiments for optimal synthesis of calcium hydroxide/ZnO/Ag nanocomposite.

Experiment	$Ca(OH)_2$ (mg/ml)			ZnO (mg/ml)			Ag (mg/ml)		
	50	100	150	1	2	3	1	2	3
1		50			1			1	
2		50			2			2	
3		50			3			3	
4		100			1			2	
5		100			2			3	
6		100			3			1	
7		150			1			3	
8		150			2			1	
9		150			3			2	

Synthesis of calcium hydroxide/ZnO/Ag nanocomposite

Using the Taguchi methodology and the Qulitek-4 software, a total of nine nanocomposites comprising calcium hydroxide, ZnO, and Ag were designed through the in situ synthesis approach for the purpose of determining their antibacterial efficacy. For this purpose, 50, 100, and 150 mg/ml of $Ca(OH)_2$ and 1, 2, and 3 mg/ml of ZnO and Ag were stirred separately by a magnetic stirrer for 60 min (Table 1). To create a uniform composition, each of the nine solutions was then dispersed by an ultrasonic homogenizer at 40°C for 20 min. Containers containing $Ca(OH)_2$ solution were placed on a magnetic stirrer and two other solutions were added dropwise and stirred for 60 min. The resulting solutions were sonicated for 20 min for complete dispersion. The resulting solutions were then dried in an oven at 80°C for 24 h [29].

Characterization

TGA, XRD, TEM, SEM, UV/-Vis, FTIR, and MAP analyses were used to identify the compositions, structure, size, and thermal behavior of NPs and nanocomposite. UV-Vis spectroscopy was performed in the range of 200-800 nm using Thermo-visible-ultraviolet spectroscopy. The FTIR spectrum was prepared from the nanocomposite and its components by FTIR spectroscopy (AVATAR model, Thermo) in the range of 400-4000 cm^{-1}. The Philips (pw1730) apparatus was employed to ascertain the dimensions and assess the crystal structure, utilizing the XRD test. By means of this analysis, diffraction patterns were attained, employing a wavelength of λ= 1.54056A0 within the angular span of (20-80) 2θ. The examination of the nanocomposite components and the structure of the nanoparticles was conducted utilizing a TESCAN MIRA3 scanning electron microscope (SEM) operating at an operating voltage of 30 kV, with various magnifications.

The structure and morphology of the synthesized nanocomposite with energy E=100 Kv/el were evaluated using a TEM made by Philips. The number of constituent elements by energy-dispersive X-ray spectroscopy (EDX) was identified by a SAMX X-ray energy detector on the SEM. Frequency distribution of elements in nanocomposite components was performed using the (X-Ray) MAP test. The thermogravimetric analysis (TGA) for calcium hydroxide/ZnO/Ag nanocomposite was performed using a TA thermal analysis device model Q600 in argon medium with a temperature increase rate of 20°C/min in the range of 25-800°C [28, 29].

Antibacterial activity

The assessment of the antibacterial effectiveness of the synthesized nanocomposite was conducted using the colony-forming unit (CFU) technique. A suspension was prepared using a brain-heart infusion (BHI) medium. To prepare a single colony of *E. faecalis*, this bacterium was cultured on a medium containing 1.5% agar and 3.85% BHI powder and incubated at 37°C for 24 h. The suspension was then prepared using distilled water twice with a concentration of 0.5 McFarland. The molar ratio of the test solution to the 1:9 suspension was added to the 96-wells plates along with adding various concentrations of the nanocomposite and incubated at 37°C for 24 h. The solution was then diluted 10 times in the wells using serial dilution and cultured in BHI medium with 1.5% (v/w %) agar and incubated at 37°C for 24 h. Then, the frequency of colonies was quantified and the mean value was computed. The experiments were replicated three times and the average value was documented.

Results and Discussion

Antibacterial analysis

The antibacterial effects of the synthesized nanocomposite components are shown in Table 2. The results showed that silver, zinc oxide NPs and calcium hydroxide had the highest antibacterial properties, respectively. The antibacterial activity of the synthesized nanocomposite against *E. faecalis* was evaluated using the Taguchi method, as shown in Fig. 1. The findings revealed that the nanocomposite synthesized under the experimental conditions 3 exhibited the most pronounced antibacterial effect. Furthermore, the nanocomposite produced under the experimental conditions 3 ($Ca(OH)_2$, ZnO, and Ag with 50, 3, and 3 mg/ml, respectively) had the greatest effect on reducing the growth of *E. faecalis* (0.29 Log_{10} CFU/ml). The lowest level of antibacterial activity (2.60 Log_{10} CFU/ml) was observed for the synthesized nanocomposite in the experimental conditions 8 (150, 2, and 1 mg/ml of $Ca(OH)_2$, ZnO, and Ag, respectively). These results are consistent with previous studies concerning the improved antimicrobial properties through nanocomposite formation [30-32].

The impact of varying degrees of the examined variables on the degree of antibacterial efficacy of the calcium hydroxide/ZnO/Ag nanocomposite is presented in Fig. 2. The results showed that level 3 of ZnO and Ag NPs and level 1 of $Ca(OH)_2$ had the highest performance in reducing the growth of *E. faecalis*. Level 3 factors of ZnO and Ag NPs reduced the viability of this bacterium by 1.00 and 1.03 Log_{10} CFU/ml, respectively, and level 1 of $Ca(OH)_2$ led to a reduction of 1.41 Log_{10} CFU/ml.

Figure 3 reports the interaction of the studied factors on the viability rate of *E. faecalis*. The third level of

Table 2. Comparison of antibacterial activity of nanocomposite calcium hydroxide/ZnO/Ag with its components.

Factors	Bacterial survival (Log_{10} CFU/ml)
$Ca(OH)_2$	3.51
ZnO	0.96
Ag	0.78
Calcium hydroxide/ZnO/Ag	0.27

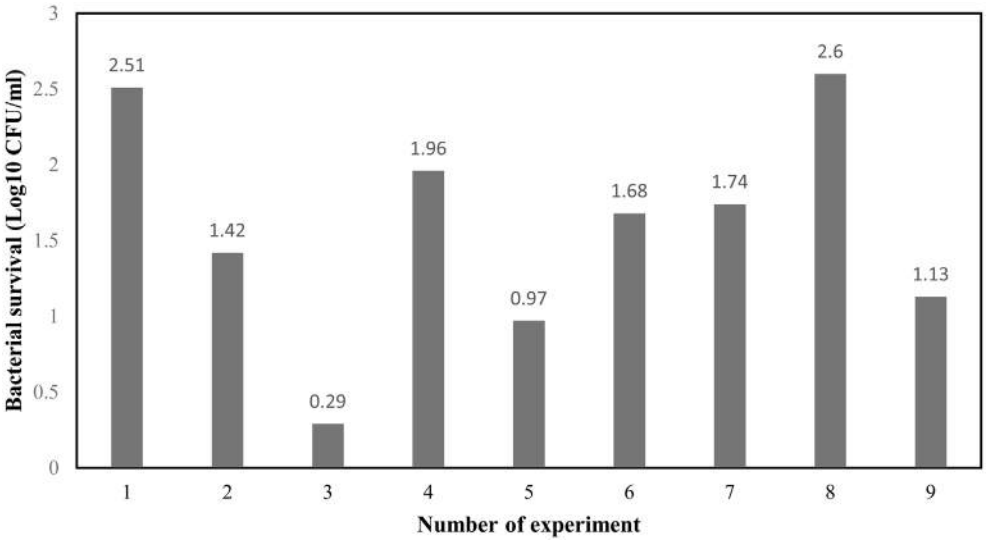

Fig. 1. Taguchi design of experiments and effects of calcium hydroxide/ZnO/Ag nanocomposite synthesized nanocomposites on the survival rate of *Enterococcus faecalis*.

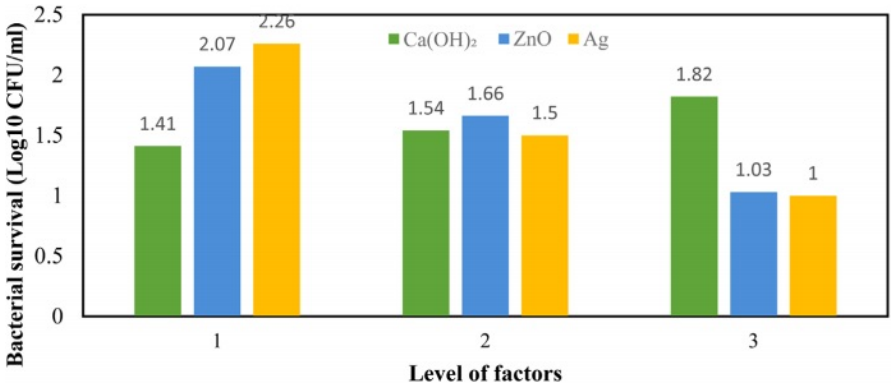

Fig. 2. The main effects of different levels of $Ca(OH)_2$, ZnO and Ag on the survival rate of *Enterococcus faecalis* (Log_{10} CFU/ml).

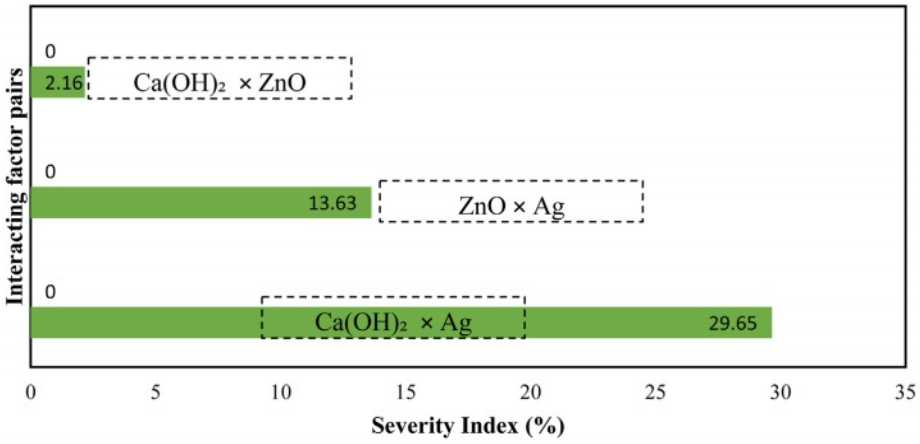

Fig. 3. The interactions effects of studied factors on the survival rate of *Enterococcus faecalis*.

$Ca(OH)_2$ and the first level of Ag showed the greatest interaction on reducing bacterial growth (29.65%). The lowest intensity of interaction (2.16%) belonged to the interaction of $Ca(OH)_2$ and ZnO in the third and first levels. These results are consistent with previous studies that showed the effectiveness of nanoparticle concentrations on the antibacterial activity of compounds containing them [28, 33].

According to the ANOVA results, ZnO and Ag NPs (with 55.52% and 37.36%, respectively) were the most

Table 3. The analysis of variance of factors affecting the survival rate of *Enterococcus faecalis*.

Factors	DOF	Sum of Squares	Variance	F-Ratio (F)	Pure Sum	Percent (%)
$Ca(OH)_2$	2	0.27	0.14	22.19	0.26	5.99
ZnO	2	1.64	0.82	133.23	1.62	37.36
Ag	2	2.43	1.21	197.52	2.41	55.52

DOF, degree of freedom.

Table 4. The optimum conditions for the synthesis of calcium hydroxide/ZnO/Ag nanocomposite with the highest antibacterial activity.

Factors	Level	Contribution
$Ca(OH)_2$	1	-0.18
ZnO	3	-0.56
Ag	3	-0.59
Total contribution from all factors		-1.33
Current grand average of performance		1.59
Bacterial survival at optimum condition		0.26

effective factors in reducing the growth of *E. faecalis*, and the least effective factor (5.99%) was $Ca(OH)_2$ (Table 3).

The findings regarding the prognostication of the most advantageous circumstances for the amalgamation of calcium hydroxide/ZnO/Ag nanocomposite, which exhibits the most elevated antibacterial efficacy, are delineated in Table 4. The Ag NP and $Ca(OH)_2$ factors respectively showed the highest and the lowest impacts on reducing bacterial viability. The third level of ZnO and Ag factors and the first level of $Ca(OH)_2$ represented the most appropriate levels; hence, it is predicted that the nanocomposite synthesized in these conditions will prevent the growth of bacteria up to 0.26 Log_{10} CFU/ml.

UV-Vis

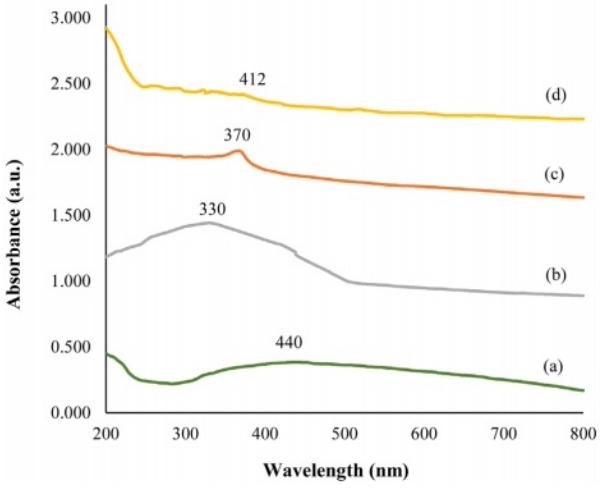

Fig. 4. UV-Visible of Ag NPs (a), Calcium Hydroxide (b), ZnO NPs (c), Calcium Hydroxide/ZnO/Ag nanocomposite (d).

Figure 4 shows the UV spectra of calcium hydroxide/ZnO/Ag nanocomposite and their components. The utilization of UV-Vis spectroscopy was employed to explore the absorption spectra of both the nanocomposite and its individual constituents. This investigation was conducted within the wavelength range of 200-800 nm. The determination of the particular wavelength at which a molecule absorbs radiation is contingent upon the magnitude of the electrons participating in its bonding. Absorptive bands were detected in the spectrums of silver nanoparticles (diagram a) and calcium hydroxide (diagram b) at wavelengths 440 and 330, correspondingly. An absorption band also formed for ZnO NPs (diagram c) at a wavelength of about 370 nm. The presence of a broad absorption peak in the absorption spectrum of UV-Vis spectroscopy for nanoparticles, along with the opacity of the peaks, demonstrates that the outcomes of UV-Vis spectra validate the data obtained from field emission scanning microscopy. These findings substantiate the distinctive and quantum attributes of nanoparticles.

FTIR analysis

Figure 5 shows the FTIR spectra of calcium hydroxide/ZnO/Ag nanocomposite and their components in the wavelength range of 400-4000 cm^{-1}. In the spectrum of Ag NPs (diagram a), the stretching vibrations of the O-H bond are observed in the region of 3413 cm^{-1}. The peaks observed in the range of 1591 and 1391 cm^{-1} are the result of vibrations caused by the C = C bond and stretching vibrations of the C-N bond, respectively. The

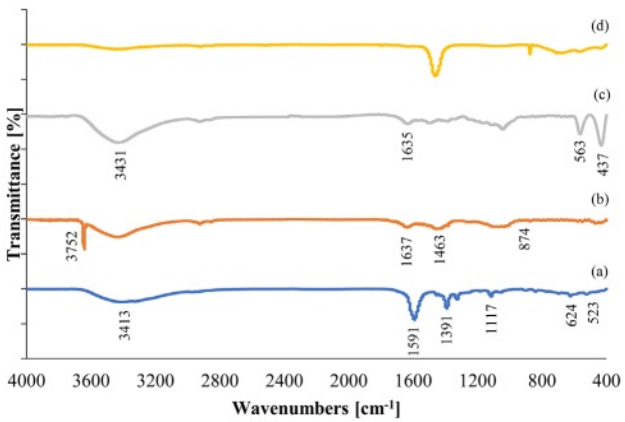

Fig. 5. Fourier-transform infrared spectroscopy of Ag NPs (a), Calcium Hydroxide (b), ZnO NPs (c), Calcium Hydroxide/ZnO/Ag nanocomposite (d).

occurrence of the maximum at 1117 cm^{-1} signifies the presence of ether bonds and the existence of compounds that have been adsorbed onto the surface of Ag NPs. On the other hand, the observed maximum within the 523 cm^{-1} range can be attributed to the existence of pure Ag NPs [27, 34].

In the relevant $Ca(OH)_2$ spectrum (diagram b), sharp peaks are observed in 364 and 3752 cm^{-1} regions due to the stretching state of the surface hydroxyl group in the FTIR spectrum. The peak observed in the absorption region of 1463 cm^{-1} belongs to the carbonate anion group of $CO3^{-2}$ calcium carbonate. The peaks observed in the 874 cm^{-1} regions result from the curved plate outside the $CO3^{-2}$ type plate relative to the $Ca(OH)_2$ network. The peak observed in the 1637 cm^{-1} region belongs to O-H vibration, which indicates the absorption of moisture and water molecules in these nanoparticles [35].

In the spectrum of ZnO NPs (diagram c), the broad peaks in the region of 3000-3680 cm^{-1} arise from the OH tensile of the remaining alcohols, water, and Zn-OH. The peak at the 1635 cm^{-1} position indicates the flexural state of the H-OH bond in ZnO NPs. The strongest absorption peak is observed in the region of 437 cm^{-1}, resulting from the vibrational tensile of oxygen (O) and zinc (Zn). Zn-O tensile bands at 437 and 563 cm^{-1} peaks correspond to pure samples of ZnO NPs [36, 37].

A comparison of the final spectrum of nanocomposite (diagram d) and their components showed that this spectrum resulted from the interaction of the components and confirmed the synthesis of this nanocomposite.

XRD analysis

Phase formation and crystallography of the samples of the nanoparticles and nanocomposite of calcium hydroxide/ZnO/Ag were investigated using the XRD analysis (Fig. 6). The crystalline behavior of nanocomposite components was investigated through the XRD analyses of Ag NPs (diagram a), $Ca(OH)_2$ (diagram b), and ZnO NPs (diagram c). The XRD pattern of Ag NPs shows a cubic crystal structure with centered dimensions for this material. The Miller indices (hkl) of

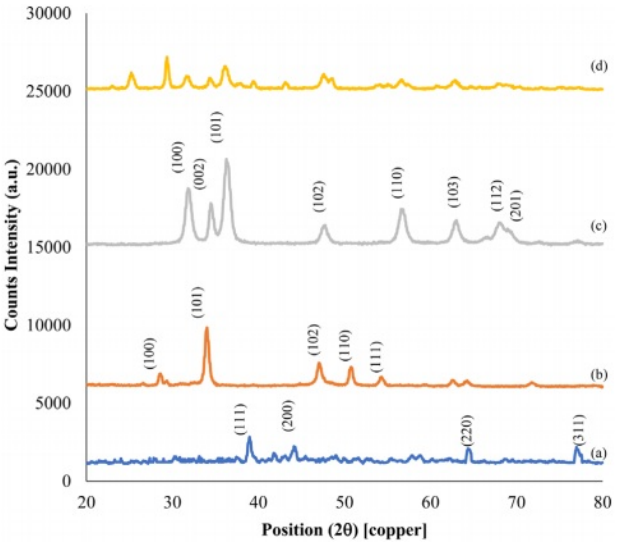

Fig. 6. XRD Pattern of Ag NPs (a), Calcium Hydroxide (b), ZnO NPs (c), Calcium Hydroxide/ZnO/Ag nanocomposite (d).

(111), (200), (220), and (311) were calculated at 39.07, 44.32, 64.62, and 77.17 angles 2θ degrees, respectively [34].

The XRD pattern of $Ca(OH)_2$ NPs showed a calcite phase with a hexagonal crystal structure for this material. Miller indices (hkl) of (100), (101), (102), (110), and (111) were calculated at 28.52, 33.95, 47.07, 50.63, and 54.22 angles θ2 degrees, respectively [38]. Average crystal size of 32 nm was also calculated for the highest peak (101) using the Debye Scherrer formula.

The XRD pattern of the ZnO NPs shows the zincite phase with hexagonal crystal structure for this material. Miller indices (hkl) of (100), (002), (102), (103), (110), (112), and (201) were calculated at 31.75, 34.54, 36.30, 47.69, 56.57, 62.96, 68.02, and 69.27 angles 2θ degrees, respectively [36].

The X-ray nanocomposite pattern derived from the calcium hydroxide/ZnO/Ag nanocomposite (diagram d) demonstrated a decrease in intensity, elimination of certain peaks, or the leveling of peaks, as well as a

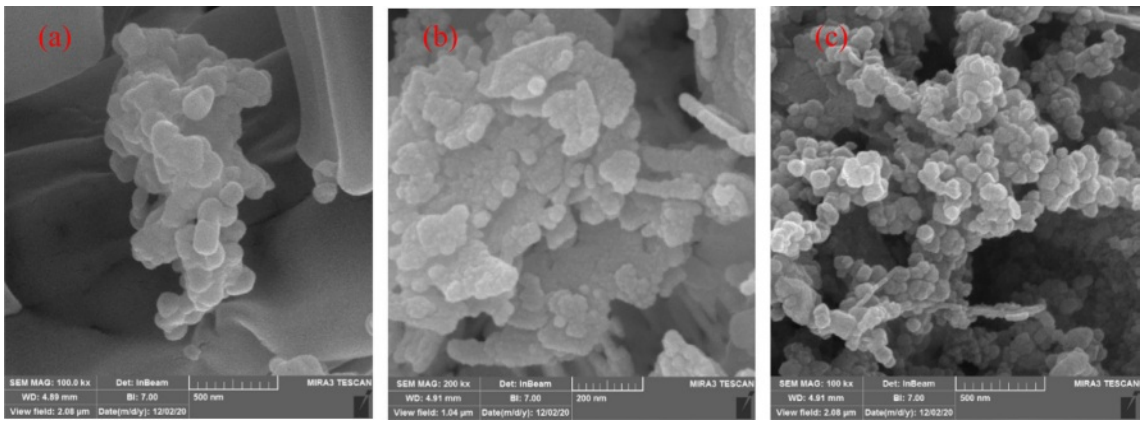

Fig. 7. The scanning electron microscope image of Ag NPs (a), ZnO NPs (b), Calcium Hydroxide/ZnO/Ag nanocomposite (c).

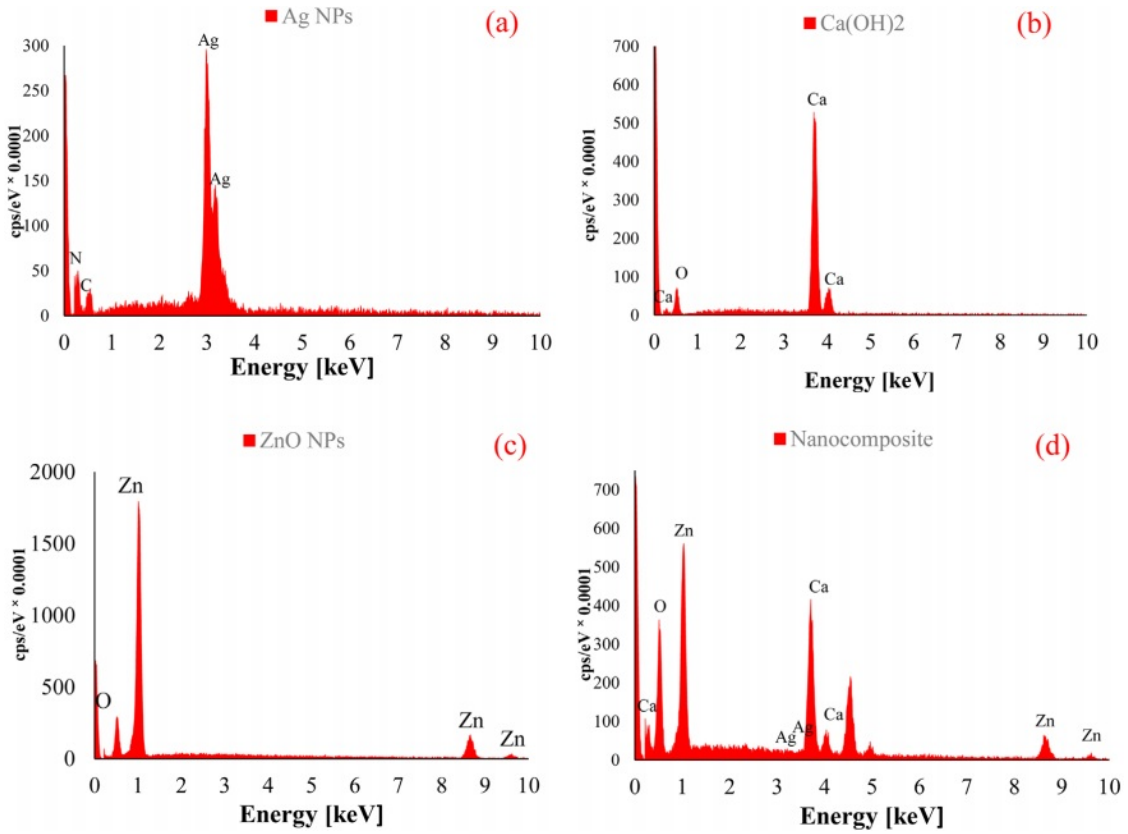

Fig. 8. The energy dispersive X-ray (EDX) pattern of Ag NPs (a), Calcium Hydroxide (b), ZnO NPs (c), Calcium Hydroxide/ZnO/Ag nanocomposite (d).

displacement to the left or right in the XRD spectrum of the synthesized nanocomposite compared to that of the individual components. The primary cause of this phenomenon can be attributed to alterations in the spatial intervals between the crystalline structures as a consequence of the unique composition of the constituent elements within the nanocomposite. This serves as an indication of the ideal arrangement and construction of the ultimate nanocomposite. Furthermore, utilizing the Debye Scherrer formula, a mean crystal size of 39 nm was determined for the most prominent peak.

SEM analysis

SEM images of nanoparticles and calcium hydroxide/ZnO/Ag nanocomposite are shown in Fig. 7. The size of nanoparticles and synthesized nanocomposites varies between 50 and 60 nm. The shape of these nanoparticles is relatively spherical.

EDX analysis

EDX spectroscopy was used to study the elemental analysis and to determine the structural elements of calcium hydroxide/ZnO/Ag nanocomposite and their components (Fig. 8). The spectrum of Ag NPs showed the presence of silver (Ag), carbon (C), and nitrogen (N) elements, which indicated a small impurity in the synthesized nanoparticles. The presence of calcium (Ca) and oxygen (O) in the spectrum of $Ca(OH)_2$ confirmed the pure structure. The presence of O and Zn in the spectrum of ZnO NPs showed a high percentage of purity in this compound. The elemental analysis outcomes of the nanocomposite, comprising calcium hydroxide, ZnO, and Ag, revealed the existence of Ca, Zn, Ag, and O elements. This observation serves as confirmation for the creation of the nanocomposite.

Map analysis

The elemental dispersion map on the surface of calcium hydroxide/ZnO/Ag nanocomposite is shown in Fig. 9. The distribution of elemental O, Ca, Zn, and Ag, as well as the distribution in the overall composition of the synthesized nanocomposite, uniformly affirms the establishment of the nanocomposite.

TEM analysis

The TEM micrograph of the calcium hydroxide/ZnO/Ag nanocomposite is shown in Fig. 10. The examination of TEM images revealed that the synthesized nanocomposite exhibited suitable dimensions, morphology. As MAP analysis confirmed the dispersion of elements in the nanocomposite structure. The results of TEM analysis also showed that the nanoparticles were effectively dispersed within the $Ca(OH)_2$ framework.

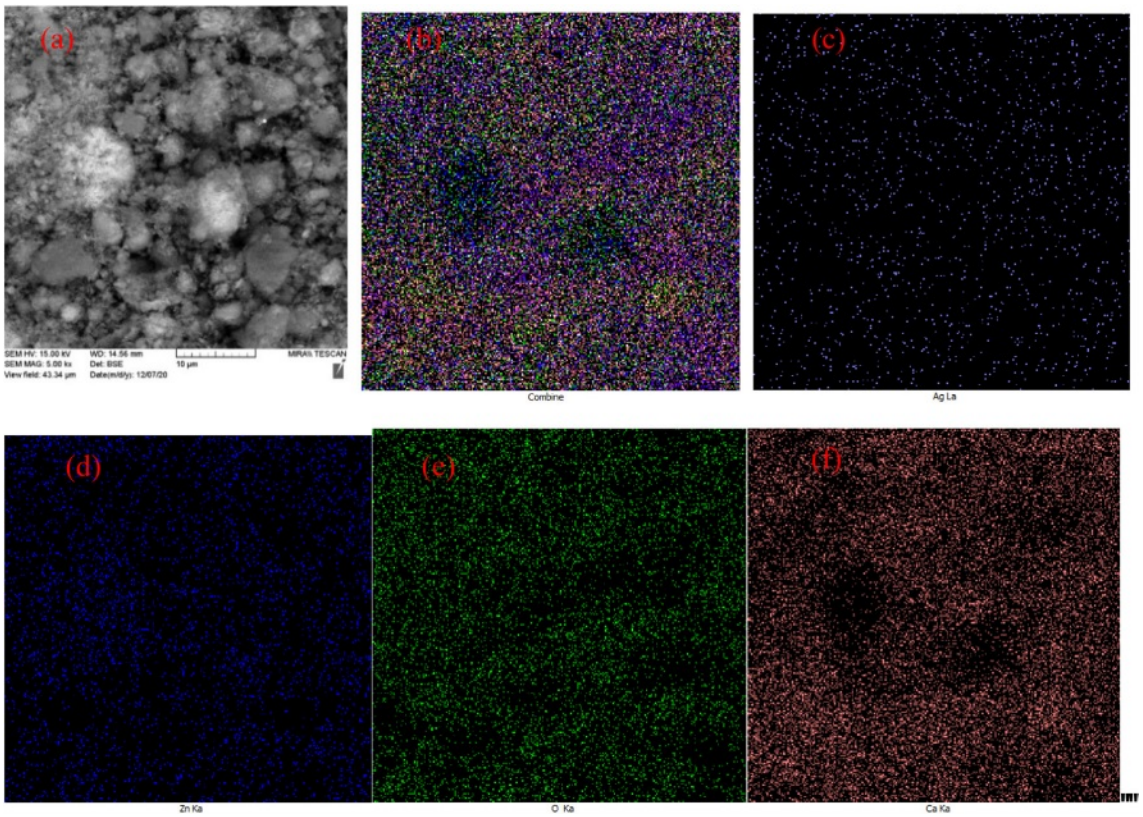

Fig. 9. Dispersion map of composition components on the surface of final nanocomposite (a), all elements (b), Silver (c), Calcium (d), Oxygen (e), Zinc (f).

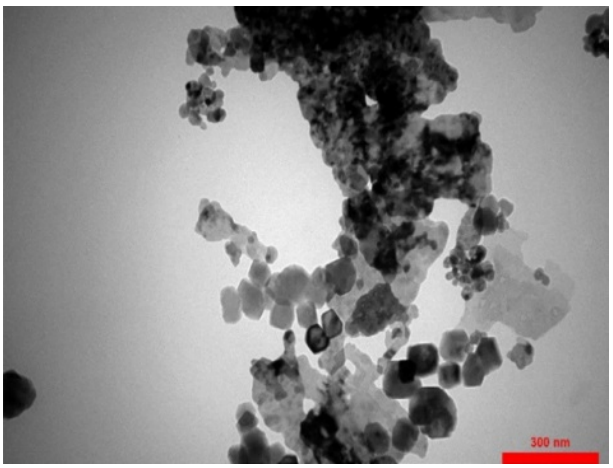

Fig. 10. The transmitted electron microscope image of Calcium Hydroxide/ZnO/Ag nanocomposite.

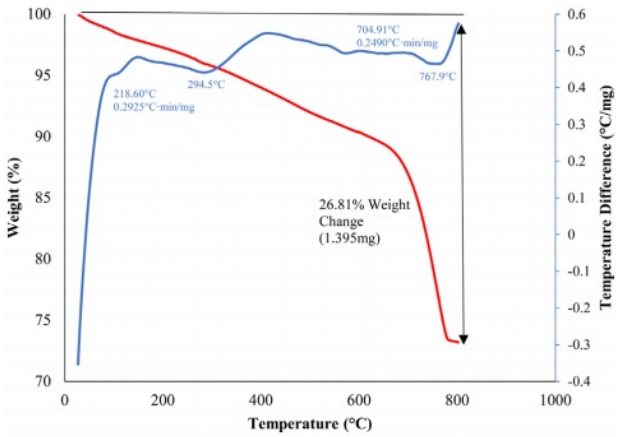

Fig. 11. Thermogravimetric analysis (TG/DTA) of Calcium Hydroxide/ZnO/Ag nanocomposite.

TGA and DTA analysis

The thermogravimetric analysis (TGA) was used to assess the resistance of the synthesized nanocomposite to high temperatures. This test was performed under argon atmosphere in the temperature range of 25-800°C. Fig. 11 shows that the 1-4% weight loss of the nanocomposite in the range of 100-300°C is due to the release of adsorbed surface moisture on the nanocomposite surface. A further weight loss of 11-16% occurred in the range of 300-420°C due to the removal of structurally bound water molecules during which $Ca(OH)_2$ is converted to calcium oxide (CaO) [38]. In differential scanning calorimeter analysis diagrams, upward and downward peaks are generally endothermic and exothermic, respectively. At temperatures above 600°C, potential impurities and by-products were destroyed by heat. By examining the TGA diagram and observing the reduction of total weight changes by 26.81%, it is possible to realize the relatively high thermal stability of this nanocomposite.

Conclusion

The optimization conditions of the calcium hydroxide/ZnO/Ag nanocomposite with the most potent antibacterial activity were ascertained by employing the Taguchi method and Qulitek-4 software, in accordance with the discoveries made in this research study. The examination of the calcium hydroxide/ZnO/Ag nanocomposite and its constituents through the application of analytical techniques such as FTIR, XRD, UV-Vis, EDX, TEM, SEM, TGA, and MAP analyses, yielded definitive evidence supporting the creation of the calcium hydroxide/ZnO/Ag nanocomposite and the enhancement of its characteristics. The compound synthesized in this study exhibits exceptional performance and possesses desirable properties, thus rendering it suitable for application as a root canal disinfectant within the field of dentistry.

Data Availability

The data used to support the findings of this study are included within the article.

Conflicts Of Interest

The authors declare that they have no conflicts of interest.

Acknowledgement

The authors gratefully acknowledge the Research Council of Kermanshah University of Medical Sciences for financial support (Grant No. 990231).

References

1. E. Giacomini, V. Perrone, D. Alessandrini, D. Paoli, C. Nappi, and L. Degli Esposti, Infect. Drug. Resist. 14 (2021) 849-858.
2. L.L. Narayanan and C. Vaishnavi, J. Conserv. Dent. 13 (2010) 233-239.
3. I.N. Rôças, J.F. Siqueira, and K.R. Santos, J. Endod. 30 (2004) 315-320.
4. M. Abdullah, Y.L. Ng, K. Gulabivala, D.R. Moles, and D.A. Spratt, J. Endod. 31 (2005) 30-36.
5. J.F. Siqueira, I.N. Rôças, and D. Ricucci, Endod. Topics. 22 (2010) 33-49.
6. A. Law and H. Messer, J. Endod. 30 (2004) 689-694.
7. A. Saafan and M.H. Zaazou, Open Access Maced. J. Med. Sci. 6 (2018) 1289-1295.
8. A.A. Husseina, M.A. Mutar, and A. Ficai. J. Ceram. Process. Res. 25 (2024) 178-191.
9. M. Ji and Y.I. Lee, J. Ceram. Process. Res. 22 (2021) 386-393.
10. R. Pavaskar, N. de Ataide Ide, P. Chalakkal, M.J. Pinto, K.S. Fernandes, R.V. Keny, and A. Kamath, J. Endod. 38 (2012) 95-101.
11. T.C. Pereira, L.R. da Silva Munhoz Vasconcelos, M.S.Z. Graeff, M.C.M Ribeiro, M.A.H. Duarte, and F.B. de Andrade, Clin. Oral. Investig. 23 (2019) 1253-1262.
12. C.H. Stuart, S.A. Schwartz, T.J. Beeson, and C.B. Owatz, J. Endod. 32 (2006) 93-98.
13. A.S. Aguiar, J.M. Guerreiro-Tanomaru, G. Faria, R.T. Leonardo, and M. Tanomaru-Filho, J. Contemp. Dent. Pract. 16 (2015) 624-629.
14. M. Safaei, H.R. Mozaffari, H. Moradpoor, M.M. Imani, R. Sharifi, and A. Golshah, Adv. Mater. Sci. Eng. 2022 (2022) 1376998.
15. M. Taran, S. Etemadi, and M. Safaei, J. Appl. Polym. Sci. 134 (2017) 44613.
16. A. Vassallo, M.F. Silletti, I. Faraone, and L. Milella, J. Nanomater. 2020 (2020) 6905631.
17. H. Moradpoor, M. Safaei, A. Golshah, H.R. Mozaffari, R. Sharifi, M.M. Imani, and M.S. Mobarakeh, Inorg. Chem. Commun. 130 (2021) 108748.
18. W. Cao and Y. Zhang, J. Mater. Sci. Mater. Med. 29 (2018) 162.
19. M. Safaei and M. Taran, Int. J. Biol. Macromol. 104 (2017) 449-456.
20. S. Iwana, D. Dianisyaa, R. F. Isnaenib, E. Budia, A. Budi Susilaa, and E. Handokoa, J. Ceram. Process. Res. 20 (2019) 518-521.
21. Y. Fu, J. Lu, J. Wang, and L. Li, J. Ceram. Process. Res. 24 (2023) 728-735.
22. N. Jones, B. Ray, K.T. Ranjit, and A.C. Manna, FEMS Microbiol. Lett. 279 (2008) 71-76.
23. A. Kishen, Z. Shi, A. Shrestha, and K.G. Neoh, J. Endod. 34 (2008) 1515-1520.
24. M.K. Rai, S.D. Deshmukh, A.P Ingle, and A.K. Gade, J. Appl. Microbiol. 112 (2012) 841-852.
25. S. Ghosh, V.S. Goudar, K.G. Padmalekha, S.V. Bhat, S.S. Indi, and H.N. Vasan, RSC Adv. 2 (2012) 930-940.
26. J. Shang, Y. Sun, T. Zhang, Z. Liu, and H. Zhang, J. Nanomater. 2019 (2019) 3281802.
27. Y. Dasaradhudu and M.A. Srinivasan, Mater. Today. Proc. 33 (2020) 720-723.
28. M. Imani, M. Kiani, F. Rezaei, R. Souri, and M. Safaei, Ceram. Int. 47 (2021) 33398-033404.
29. A. Moghadam, M.S. Mobarakeh, M. Safaei, and S. Kariminia, Carbohydr. Polym. 260 (2021) 117802.
30. D. Paul, S. Maiti, D.P. Sethi, and S. Neogi, Adv. Powder Technol. 32 (2021) 131-143.
31. M.D. Firouzjaei, A.A. Shamsabadi, G.M. Sharifian, A. Rahimpour, and M. Soroush, Adv. Mater. Interfaces. 5 (2018) 1701365.
32. M. Safaei, M. Taran, M.M. Imani, H. Moradpoor, F. Rezaei, L. Jamshidy, and R. Rezaei, Pol. J. Chem. Technol. 21 (2019) 116-122.
33. N.T. Vo, M.Q. Do, and V. Van Pham, J. Aust. Ceram. Soc. 59 (2023) 1205-1212.
34. K. Anandalakshmi, J. Venugobal, and V. Ramasamy, Appl. Nanosci. 6 (2016) 399-408.
35. K. Karthik, S. Dhanuskodi, C. Gobinath, S. Prabukumar, and S. Sivaramakrishnan, J. Mater. Sci.: Mater. Electron. 28 (2017) 16509-16518.
36. P.G. Devi and A.S. Velu, J. Theor. Appl. Phys. 10 (2016) 233-240.
37. F. Ghorbani, P. Gorji, M.S. Mobarakeh, H.R. Mozaffari, R. Masaeli, and M. Safaei, J. Nanomater. 2022 (2022) 7255181.
38. A. Samanta, S. Podder, C.K. Ghosh, M. Bhattacharya, J. Ghosh, A.K. Mallik, A. Dey, and A.K. Mukhopadhyay, J. Mech. Behav. Biomed. Mater. 72 (2017) 110-128.